ELSEVIER

International Journal of Heat and Fluid Flow 23 (2002) 831–839

International Journal of HEAT AND FLUID FLOW

www.elsevier.com/locate/ijhff

Mixed convection boundary layer flow of non-Newtonian fluids along vertical wavy plates

Chi-Chang Wang, Cha'o-Kuang Chen *

Department of Mechanical Engineering, National Cheng Kung University, Tainan 701, Taiwan ROC

Received 23 March 2001; accepted 21 December 2001

Abstract

Mixed convection boundary layer flows of non-Newtonian fluids over the wavy surfaces are studied by the coordinate transformation and the cubic spline collocation numerical method. The effects of the wavy geometry, the buoyancy parameter and the generalized Prandtl number for pseudoplastic fluids, Newtonian fluids and dilatant fluids on the skin-friction coefficient, local and mean Nusselt numbers have been graphically studied. Results show that both higher generalized Prandtl numbers and buoyancy parameters are seen to enhance the influence of wavy surfaces on the local Nusselt number, irrespective of whether the fluids are Newtonian fluids or non-Newtonian fluids. Moreover, the irregular surfaces have higher total heat flux than that of corresponding flats plate for any fluid.

Keywords: Mixed convection; Non-Newtonian fluids; Wavy surface; Cubic spline

1. Introduction

In recent years, non-Newtonian fluids have received much attention because many practical applications are not in traditional Newtonian fluids. Most of the previous studies have focused mainly on the heat transfer characteristics for non-Newtonian fluids flow over flat plates (see, for example, Lloyd and Sparrow, 1970, Huang and Chen, 1984, Wang, 1995, Hady, 1995, and the references cited therein). However, irregular surfaces frequently occur in the process of manufacture even though the complex boundary conditions or external flow fields are difficult to deal with. Moreover, surfaces are sometimes intentionally roughened to enhance heat transfer for the presence of rough surfaces disturbs the flow and alters the heat transfer rate. In the following, some previous works done on wavy surfaces will be discussed.

The natural convection heat transfer along vertical wavy surfaces (i.e. sinusoidal surfaces) has been studied by Moulic and Yao (1989a,b) and Rees and Pop (1994) for Newtonian fluids; Chiu and Chou (1994) for micropolar fluids; Kim (1997) and Kumari et al. (1997) for non-Newtonian fluids. In general, it has been found that the local heat transfer rate varies periodically along the wavy surface, with a frequency equal to twice the frequency of the wavy surface. On the other hand, these investigations into mixed convection of Newtonian fluids along a vertical wavy surface are carried out by Moulic and Yao (1989a,b). Numerical results show that the axial distribution of the local Nusselt number shows a mixture of two harmonics. The amplitude of the first harmonic is proportional to that of the wavy surface, and the natural-convection component is the second harmonic with a frequency twice that of the wavy surface. Recently, Pop et al. (1996) investigate the forced convection boundary layer flow of power-law fluids over wavy surfaces. They find that the skin-friction coefficient decreases with the power-law index increased. Furthermore, the rise and fall of the skin-friction coefficient is seen to follow the change of the surface contour.

The above literature survey shows that the combined free and forced convection of non-Newtonian fluids along irregular surfaces in laminar boundary layer flow has not been studied so far. In this study, a simple coordinate transformation is employed to transform a complex wavy surface to a flat plate, and the cubic spline

* Corresponding author. Tel.: +886-6-275-7575; fax: +886-6-234-2081.

E-mail address: ckchen@mail.ncku.edu.tw (C.-K. Chen).

0142-727X/02/$ - see front matter © 2002 Published by Elsevier Science Inc.
PII: S0142-727X(02)00145-5

Nomenclature

a	amplitude of wavy surface
C_f	skin-friction coefficient
C_p	specific heat of the fluid at constant pressure
g	gravitational acceleration
Gr	generalized Grashof number
h	heat transfer coefficient
J	second invariant of the strain-rate tensor
K	fluid consistency index for power-law fluid
K_f	thermal conductivity
L	characteristic length
Nu_x	local Nusselt number
Nu_m	mean Nusselt number
n	power-law viscosity index
p	pressure
Pr	generalized Prandtl number
Re	generalized Reynolds number
Ri	Richardson number
S	surface geometry function
U_w	x component of the velocity of the inviscid flow, evaluated at the wavy surface
T	temperature
u, v	x and y components of velocity, respectively
x, y	coordinates

Greeks

α	wavy amplitude–wavelength ratio
σ	distance measured along the surface from the leading edge
θ	dimensionless temperature
ρ	density of fluid
η	coordinate
ψ	stream function

Subscripts

w	wall surface
∞	free stream condition

Superscripts

$-$	dimensional variables
$\sim$, $\wedge$	dimensionless quantities
$'$	derivative with respect to x

collocation method is then used to solve the flow patterns and heat transfer characteristics. The effects of the wavy geometry, the power-law viscosity index, the Richardson number and the generalized Prandtl number on the skin-friction coefficient and the Nusselt number have been examined in detail. These results are also compared with the corresponding flow in Newtonian fluids.

2. Mathematical formulation

Consider steady laminar boundary layer flow of non-Newtonian fluids past semi-infinite symmetric body with a wavy surface at uniform wall temperature. The physical model and coordinate system are shown in Fig. 1, where the axis of symmetry is aligned with the oncoming uniform stream. In particular, we assume that the wavy surface is described by $S(\bar{x}) = \bar{a}\sin^2(\pi\bar{x}/L)$, where $\bar{a}$ is the amplitude of the wavy surface. By employing

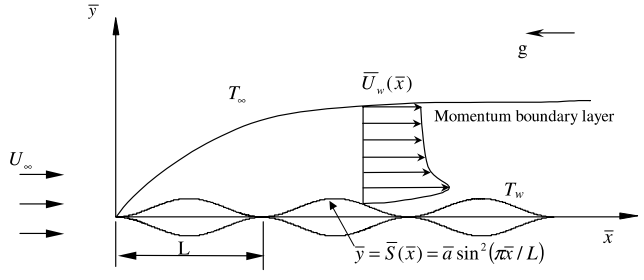

Fig. 1. Physical model and coordinate system.

the Boussinesq approximation and making use of the power-law viscosity model, the governing equations for mixed convection flow under consideration can be written in the following form:

$$\frac{\partial \bar{u}}{\partial \bar{x}} + \frac{\partial \bar{v}}{\partial \bar{y}} \tag{1}$$

$$\rho\left(\bar{u}\frac{\partial \bar{u}}{\partial \bar{x}} + \bar{v}\frac{\partial \bar{u}}{\partial \bar{y}}\right) = -\frac{\partial \bar{p}}{\partial \bar{x}} + \rho g\beta(T - T_\infty) + K\left(2\frac{\partial}{\partial \bar{x}}\left(\bar{J}\frac{\partial \bar{u}}{\partial \bar{x}}\right) + \frac{\partial}{\partial \bar{y}}\left(\bar{J}\left(\frac{\partial \bar{u}}{\partial \bar{y}} + \frac{\partial \bar{v}}{\partial \bar{x}}\right)\right)\right) \tag{2}$$

$$\rho\left(\bar{u}\frac{\partial \bar{v}}{\partial \bar{x}} + \bar{v}\frac{\partial \bar{v}}{\partial \bar{y}}\right) = -\frac{\partial \bar{p}}{\partial \bar{y}} + K\left(2\frac{\partial}{\partial \bar{y}}\left(\bar{J}\frac{\partial \bar{v}}{\partial \bar{y}}\right) + \frac{\partial}{\partial \bar{x}}\left(\bar{J}\left(\frac{\partial \bar{u}}{\partial \bar{y}} + \frac{\partial \bar{v}}{\partial \bar{x}}\right)\right)\right) \tag{3}$$

$$\rho C_p\left(\bar{u}\frac{\partial T}{\partial \bar{x}} + \bar{v}\frac{\partial T}{\partial \bar{y}}\right) = K_f\left(\frac{\partial^2 T}{\partial \bar{x}^2} + \frac{\partial^2 T}{\partial \bar{y}^2}\right) \tag{4}$$

where K is the parameter of power-law viscosity model. $\bar{J}$ is the second invariant of the strain-rate tensor and is given by

$$\bar{J} = \left\{2\left(\frac{\partial \bar{u}}{\partial \bar{x}}\right)^2 + 2\left(\frac{\partial \bar{v}}{\partial \bar{y}}\right)^2 + \left(\frac{\partial \bar{u}}{\partial \bar{y}} + \frac{\partial \bar{v}}{\partial \bar{x}}\right)^2\right\}^{(n-1)/2} \tag{5}$$

The associated boundary conditions of Eqs. (1)–(4) are

(a) On the wavy surface

$$T = T_w, \quad \bar{u} = \bar{v} = 0 \tag{6}$$

(b) Matching with the free stream

$$T \to T_\infty, \quad \bar{u} \to \overline{U}_w(\bar{x}), \quad \bar{p} \to \bar{p}_\infty(\bar{x}) \tag{7}$$

Here $\overline{U}_w(\bar{x})$ is the $\bar{x}$ component of the inviscid velocity at the free surface $\bar{y} = \bar{S}(\bar{x})$.

New, the following dimensionless variables are defined as

$$\begin{aligned}
&\tilde{x} = \frac{\bar{x}}{L} \quad \tilde{y} = \frac{\bar{y}}{L} \quad \alpha = \frac{\bar{a}}{L} \quad S = \frac{\bar{S}}{L} \\
&\tilde{u} = \frac{\bar{u}}{U_\infty} \quad \tilde{v} = \frac{\bar{v}}{U_\infty} \quad \theta = \frac{T - T_\infty}{T_w - T_\infty} \quad U_w = \frac{\bar{u}_w}{U_\infty} \quad \tilde{p} = \frac{\bar{p}}{\rho U_\infty^2} \\
&Re = \frac{\rho U_\infty^{2-n} L^n}{K} \quad Gr = \frac{g\beta(T_w - T_\infty)\rho^2 L^{1+2n} U_\infty^{2(1-n)}}{K^2} \\
&Ri = \frac{Gr}{Re^2} \\
&Pr = \frac{C_p K^{2/(n+1)}}{K_f} \left(\frac{\rho U_\infty^3}{L}\right)^{(n-1)/(n+1)}
\end{aligned} \tag{8}$$

Substituting (8) into Eqs. (1)–(5), we obtain following dimensionless equations:

$$\frac{\partial \tilde{u}}{\partial \tilde{x}} + \frac{\partial \tilde{v}}{\partial \tilde{y}} = 0 \tag{9}$$

$$\tilde{u}\frac{\partial \tilde{u}}{\partial \tilde{x}} + \tilde{v}\frac{\partial \tilde{u}}{\partial \tilde{y}} = -\frac{\partial \tilde{p}}{\partial \tilde{x}} + Ri\theta + \frac{1}{Re}\left(2\frac{\partial}{\partial \tilde{x}}\left(\tilde{J}\frac{\partial \tilde{u}}{\partial \tilde{x}}\right) + \frac{\partial}{\partial \tilde{y}}\left(\tilde{J}\left(\frac{\partial \tilde{u}}{\partial \tilde{y}} + \frac{\partial \tilde{v}}{\partial \tilde{x}}\right)\right)\right) \tag{10}$$

$$\tilde{u}\frac{\partial \tilde{v}}{\partial \tilde{x}} + \tilde{v}\frac{\partial \tilde{v}}{\partial \tilde{y}} = -\frac{\partial \tilde{p}}{\partial \tilde{y}} + \frac{1}{Re}\left(2\frac{\partial}{\partial \tilde{y}}\left(\tilde{J}\frac{\partial \tilde{v}}{\partial \tilde{y}}\right) + \frac{\partial}{\partial \tilde{x}}\left(\tilde{J}\left(\frac{\partial \tilde{u}}{\partial \tilde{y}} + \frac{\partial \tilde{v}}{\partial \tilde{x}}\right)\right)\right) \tag{11}$$

$$\tilde{u}\frac{\partial \theta}{\partial \tilde{x}} + \tilde{v}\frac{\partial \theta}{\partial \tilde{y}} = \frac{1}{Re^{2/(n+1)}Pr}\left(\frac{\partial^2 \theta}{\partial \tilde{x}^2} + \frac{\partial^2 \theta}{\partial \tilde{y}^2}\right) \tag{12}$$

where

$$\tilde{J} = \left\{2\left(\frac{\partial \tilde{u}}{\partial \tilde{x}}\right)^2 + 2\left(\frac{\partial \tilde{v}}{\partial \tilde{y}}\right)^2 + \left(\frac{\partial \tilde{u}}{\partial \tilde{y}} + \frac{\partial \tilde{v}}{\partial \tilde{x}}\right)^2\right\}^{(n-1)/2} \tag{13}$$

The next step is to transform the irregular wavy surface into a flat surface by using the following transformation

$$\begin{aligned}
&\hat{x} = \tilde{x}, \quad \hat{y} = (\tilde{y} - S)Re^{1/(n+1)} \\
&\hat{u} = \tilde{u}, \quad \hat{v} = (\tilde{v} - S'\tilde{u})Re^{1/(n+1)}, \quad \hat{p} = \tilde{p} - \tilde{p}_\infty
\end{aligned} \tag{14}$$

By substituting Eq. (14) into Eqs. (9)–(13) and under the assumption of a larger generalized Reynolds number (i.e. boundary layer approximation), the governing equations are transformed from an irregular wavy surface into a flat surface. Thus, the transformed boundary layer equations can be given as

$$\frac{\partial \hat{u}}{\partial \hat{x}} + \frac{\partial \hat{v}}{\partial \hat{y}} = 0 \tag{15}$$

$$\hat{u}\frac{\partial \hat{u}}{\partial \hat{x}} + \hat{v}\frac{\partial \hat{u}}{\partial \hat{y}} = -\frac{\partial \hat{p}}{\partial \hat{x}} + Ri\theta + Re^{1/(n+1)}S'\frac{\partial \hat{p}}{\partial \hat{y}} + (1 + S'^2)^n \frac{\partial}{\partial \hat{y}}\left(\frac{\partial \hat{u}}{\partial \hat{y}}\left|\frac{\partial \hat{u}}{\partial \hat{y}}\right|^{n-1}\right) \tag{16}$$

$$S''\hat{u}^2 + S'Ri\theta = S'\frac{\partial \hat{p}}{\partial \hat{x}} - Re^{1/(n+1)}(1 + S'^2)\frac{\partial \hat{p}}{\partial \hat{y}} \tag{17}$$

$$\hat{u}\frac{\partial \theta}{\partial \hat{x}} + \hat{v}\frac{\partial \theta}{\partial \hat{y}} = \frac{1}{Pr}(1 + S'^2)\frac{\partial^2 \theta}{\partial \hat{y}^2} \tag{18}$$

Eq. (17) indicates that the pressure gradient along y-direction is $O(Re^{-1/(n+1)})$. Therefore, from the inviscid flow solution, we can express the pressure gradient along x-direction as

$$\frac{\partial \hat{p}}{\partial \hat{x}} = -(1 + S'^2)U_w U_w' + S'S''U_w^2 \tag{19}$$

The transformed momentum Eqs. (16) and (17) can be combined into one equation by eliminating the pressure gradient $\partial\hat{p}/\partial\hat{y}$, and so, we have

$$\hat{u}\frac{\partial \hat{u}}{\partial \hat{x}} + \hat{v}\frac{\partial \hat{u}}{\partial \hat{y}} = \frac{1}{1 + S'^2}\left(-\frac{\partial \hat{p}}{\partial \hat{x}} + Ri\theta - S'S''\hat{u}^2\right) + (1 + S'^2)^n \frac{\partial}{\partial \hat{y}}\left(\frac{\partial \hat{u}}{\partial \hat{y}}\left|\frac{\partial \hat{u}}{\partial \hat{y}}\right|^{n-1}\right) \tag{20}$$

In order to remove the singularity at $x = 0$, the boundary layer equations are further transformed by means of the following variables:

$$\begin{aligned}
&x = \hat{x}, \quad y = \hat{y}\left(\frac{2\hat{x}}{U_w}\right)^{-1/(n+1)} \\
&u = \frac{\hat{u}}{U_w}, \quad v = \hat{v}\left(\frac{2\hat{x}}{U_w}\right)^{1/(n+1)}
\end{aligned} \tag{21}$$

Substituting (21) into Eqs. (15), (20) and (18) yields

$$2x\frac{\partial u}{\partial x} - \frac{2}{n+1}y\left(1 - x\frac{U_w'}{U_w}\right)\frac{\partial u}{\partial y} + \left(\frac{2x}{U_w}\right)^{(n-1)/(n+1)}\frac{\partial v}{\partial y} + 2x\frac{U_w'}{U_w}u = 0 \tag{22}$$

$$2xu\frac{\partial u}{\partial x}+\left[\left(\frac{2x}{U_w}\right)^{(n-1)/(n+1)}v-\frac{2yu}{1+n}\left(1-x\frac{U_w'}{U_w}\right)\right]\frac{\partial u}{\partial y}+2x(u^2-1)\left(\frac{S'S''}{1+S'^2}+\frac{U_w'}{U_w}\right)=\frac{2x}{U_w^2(1+S'^2)}Ri\theta+(1+S'^2)^nU_w^{n-1}\frac{\partial}{\partial y}\left(\frac{\partial u}{\partial y}\left|\frac{\partial u}{\partial y}\right|^{n-1}\right) \tag{23}$$

$$2xu\frac{\partial\theta}{\partial x}+\left[\left(\frac{2x}{U_w}\right)^{(n-1)/(n+1)}v-\frac{2yu}{1+n}\left(1-x\frac{U_w'}{U_w}\right)\right]\frac{\partial\theta}{\partial y}=\frac{1+S'^2}{Pr}\left(\frac{2x}{U_w}\right)^{(n-1)/(n+1)}\frac{\partial^2\theta}{\partial y^2} \tag{24}$$

The corresponding boundary conditions are

$$\theta=1,\quad u=v=0 \text{ as } y=0 \tag{25}$$

$$\theta\to 0,\quad u\to 1 \text{ as } y\to\infty \tag{26}$$

The last step is to obtain the surface velocity $U_w(x)$ (a necessary boundary condition). In studies of Moulic and Yao (1989a,b) and Pop et al. (1996), the velocity of the inviscid flow in the wavy surface is obtained by expressing the stream function as a two-term series, which have good results for small amplitude of wavy surface. In the present study, in order to give more accurate solution for larger wavy amplitude–wavelength ratio, the transformed coordinate and the numerical method (SOR) have been used to solve the potential flow and to determine the surface velocity U_w. Therefore, the streamline equation and the transformed coordinate can be written as following:

$$\frac{\partial^2\psi}{\partial\tilde{x}^2}+\frac{\partial^2\psi}{\partial\tilde{y}^2}=0 \tag{27}$$

$$x=\tilde{x},\quad \eta=\tilde{y}-\tilde{S}(\tilde{x}) \tag{28}$$

Substituting Eq. (28) into Eq. (27), we can get the transformed equation and the velocity $U_w(x)$, i.e.

$$\frac{\partial^2\psi}{\partial x^2}-S''\frac{\partial\psi}{\partial\eta}-2S'\frac{\partial^2\psi}{\partial x\,\partial\eta}+(1+S'^2)\frac{\partial^2\psi}{\partial\eta^2}=0 \tag{29}$$

and

$$U_w=\left.\frac{\partial\psi}{\partial\eta}\right|_{\eta=0} \tag{30}$$

The streamlines for $\alpha=0.3$ and the axial distribution of the inviscid surface velocity $U_w(x)$ and the pressure gradient (see Eq. (19)) are shown in Figs. 2 and 3, respectively. The inviscid surface velocity shows the periodical variation along the wavy surface with a cycle equals that of the surface. The flow accelerates along the portion of the surface from trough to crest, where the slope S' is positive and the pressure gradient is negative; while it decelerates along the portion of the surface from crest to trough, where the slope S' is negative and the pressure gradient is positive. Moreover, as the wavy amplitude–wavelength ratio increases, the velocity at the crest is seen to increase steadily; while at the trough the velocity is seen to decrease leisurely and then approaches zero.

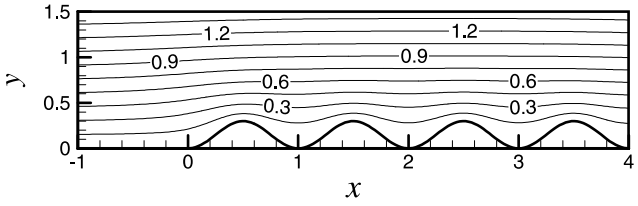

Fig. 2. Streamlines of flow for $\alpha=0.3$.

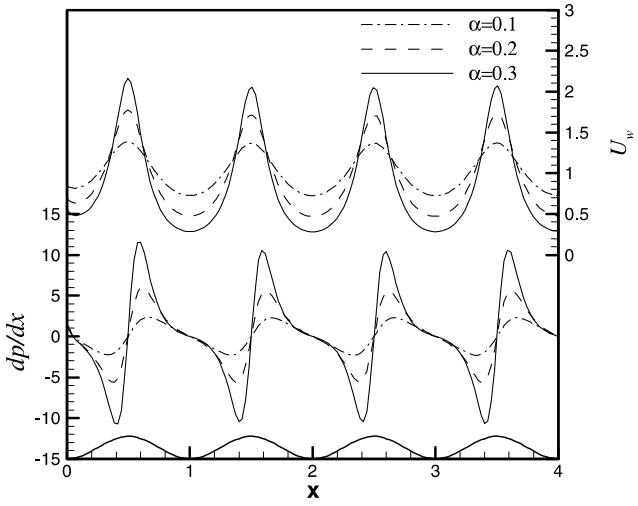

Fig. 3. Axial distribution of inviscid surface velocity and pressure gradient.

Since the flow and the temperature fields have been obtained, two important quantities can be calculated as presented below. The local Nusselt number is defined as

$$Nu_{\bar{x}}=\frac{h_{\bar{x}}\bar{x}}{K_f} \tag{31}$$

Using Newton's law of cooling and Fourier's law in Eq. (31), the local Nusselt number can be expressed as

$$\left(\frac{4}{Gr_{\bar{x}}}\right)^{1/2(n+1)}Nu_{\bar{x}}=-\left(\frac{1}{Rix}\right)^{1/2(n+1)}U_w^{1/(n+1)}\times(1+S'^2)^{1/2}\left.\frac{\partial\theta}{\partial y}\right|_{y=0} \tag{32}$$

The skin-friction coefficient C_f is defined as

$$C_f=\frac{2\tau_w}{\rho U_\infty^2} \tag{33}$$

Then the quantity of $(2Re_{\bar{x}})^{1/(n+1)}C_f$ can be expressed as

$$(2Re_{\bar{x}})^{1/(n+1)}C_f=2^{2/(n+1)}U_w^{n(n+2)/(n+1)}(1+S'^2)^n\left(\frac{\partial u}{\partial y}\right)^n \tag{34}$$

When $Ri \neq 0$ the skin-friction coefficient can also be expressed as

$$Ri^{-1}\left(\frac{Gr}{2(n+1)x}\right)^{1/2(n+1)} C_f = \left(\frac{n+1}{2}\right)^{-1/2(n+1)} \times \left(\frac{1}{Rix}\right)^{(2n+1)/2(n+1)} U_w^{n(n+2)/(n+1)}(1+S^{'2})^n \left(\frac{\partial u}{\partial y}\right)^n \tag{35}$$

3. Numerical method

The coupled Eqs. (22)–(24) and associated boundary conditions were solved by using the cubic spline collocation procedure (Rubin and Graves, 1975; Wang and Kahawita, 1983). Using the spline formulation and the false transient technique, we can write the governing differential equations in the following form:

$$\varphi_{i,j}^{z+1} = F_{i,j} + G_{i,j}\left(\frac{\partial \varphi}{\partial y}\right)_{i,j}^{z+1} + S_{i,j}\left(\frac{\partial^2 \varphi}{\partial y^2}\right)_{i,j}^{z+1} \tag{36}$$

where i and j refer to the computational nodes, z is the time step, φ represents u or θ. $F_{i,j}$, $G_{i,j}$ and $S_{i,j}$ are the known coefficients evaluated at the previous time step. Furthermore, by using cubic spline collocation relations described in Rubin and Graves (1975), Eq. (36) may be written in tri-diagonal form as

$$A_{i,j}\Omega_{i,j}^{n+1} + B_{i,j}\Omega_{i,j}^{n+1} + C_{i,j}\Omega_{i,j}^{n+1} = D_{i,j} \tag{37}$$

where Ω represents u or θ, or its first and second derivatives. The Thomas algorithm is then employed to solve Eq. (37).

Since the singularity at $x = 0$ has been removed by the scaling, the computation starts from $x = 0$, and then marches downstream. At every x-station, the iteration process continues until the convergence criterion is achieved

$$\left|\frac{\Omega_{i,j}^{n+1} - \Omega_{i,j}^{n}}{\Omega_{i,j}^{n+1}}\right| \leqslant 1 \times 10^{-5} \tag{38}$$

4. Results and discussion

Since the spline alternating-direction implicit method can evaluate the spatial derivative terms directly without any finite difference discretization and the requirement of a uniform mesh is not necessary. Therefore, the present work employs 150×50 non-uniform grids with smaller spacing mesh points near the fluid–solid boundary at y-direction and near the leading edge at x-direction. The independence of results from mesh densities has been successfully checked by repeated calculations with finer meshes. In order to verify the numerical accuracy of solutions, numerical results have been shown in Table 1 for the case of a flat plate ($\alpha = 0$) immersed in a Newtonian fluid (i.e. $n = 1.0$) with different Prandtl numbers and boundary parameters Gr_x/Re_x^2. In all cases, the local Nusselt number $Re_{\bar{x}}^{-1/2}Nu_{\bar{x}}$ is found to be in excellent agreement with those of Lloyd and Sparrow (1970) and Wang (1995). Table 2 also compares the local skin-friction coefficient $(2Re_{\bar{x}})^{1/(n+1)}C_f$ for forced convection flow along a flat plate in non-Newtonian fluids. It is seen that the data calculated by Eq. (34) has little discrepancy compared with that of Huang and Chen (1984) for $n = 0.5$ and 1.5. However, the data set matches very well with Wang (1995) for any power-law viscosity index.

Numerical results have been obtained for the surface described by $S(\bar{x}) = \bar{a}\sin^2(\pi\bar{x}/L)$, or $S(x) = \alpha\sin^2(\pi x)$, for wavy amplitude–wavelength ratios $\alpha = 0.0$ (flat plate), 0.1 and 0.2. The power-law model is used for non-Newtonian fluids with exponent $n < 1$ for pseudoplastic fluids; $n = 1$ for Newtonian fluids; and $n > 1$ for dilatant fluids. The influence of governing physical parameters such as generalized Prandtl number and buoyancy parameter (i.e. Richardson number, Ri) is explored for a wide range. Figs. 4 and 5 show the three-dimensional plots of axial velocity component u for $n = 0.5$ (pseudoplastic fluids) and $n = 1.5$ (dilatant fluids) at $\alpha = 0.2$, $Ri = 10$ and $Pr = 1$, respectively. Clearly, forced convection is the dominant mode of heat transfer near the leading edge, while further downstream, free convection becomes the dominant mode of heat transfer due to the increase of buoyancy. It is also seen that the hydrodynamic boundary layer thicknesses for $n = 0.5$ is

Table 1
Comparison of $Re_{\bar{x}}^{-1/2}Nu_{\bar{x}}$ for mixed convection of Newtonian fluids (i.e. $n = 1$) along a vertical flat plate

Gr_x/Re_x^2	$Pr = 0.72$			$Pr = 100$		
	Lloyd and Sparrow (1970)	Wang (1995)	Present method	Lloyd and Sparrow (1970)	Wang (1995)	Present method
0.00	0.2956	0.29550	0.2957	1.572	1.5708	1.5732
0.04	0.3044	0.29801	0.3050	1.585	1.5891	1.5899
0.10	0.3158	0.30502	0.3171	1.606	1.6152	1.6159
0.40	0.3561	0.36097	0.3600	1.691	1.7273	1.7269
1.00	0.4058	0.41441	0.4128	1.826	1.8959	1.8950

Table 2
Comparison of $(2Re_{\bar{x}})^{1/(n+1)}C_f$ for forced convection of non-Newtonian fluids along a flat plate

	n				
	0.5	0.8	1.0	1.2	1.5
Huang and Chen (1984)	1.8439	1.1916	0.9390	0.76191	0.5814
Wang (1995)	1.8290	1.1911	0.9390	0.76137	0.5808
Present method	1.8288	1.1899	0.9389	0.76176	0.5802

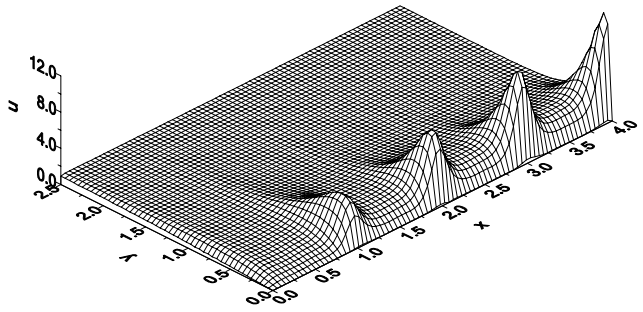

Fig. 4. Axial velocity distribution for $n = 0.5$, $\alpha = 0.2$, $Ri = 10$ and $Pr = 1$.

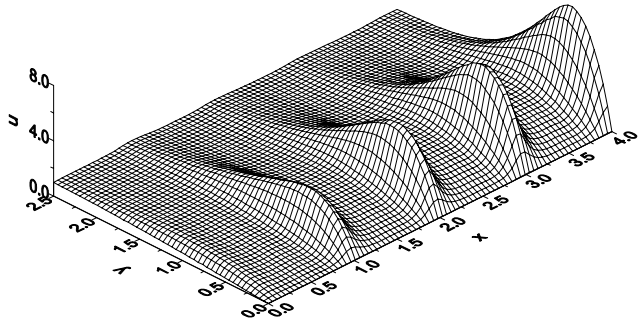

Fig. 5. Axial velocity distribution for $n = 1.5$, $\alpha = 0.2$, $Ri = 10$ and $Pr = 1$.

smaller than that for $n = 1.5$ ever if both hydrodynamic boundary layer thickness reduce with x.

Figs. 6 and 7 show the axial distributions of the local Nusselt number $(4/Gr_{\bar{x}})^{1/2(n+1)}Nu_{\bar{x}}$ and the local skin-fiction coefficient $Ri^{-1}(Gr/2(n+1)x)^{1/2(n+1)}C_f$ for $\alpha = 0.2$, $Ri = 10$ and $Pr = 1$, including results of the limiting case of a flat plate ($\alpha \to 0$) for comparison. In Fig. 6, It is observed that the dilatant fluids ($n = 1.5$) has larger local Nusselt number than that of the Newtonian fluids ($n = 1$) and the pseudoplastic fluids ($n = 0.5$) near the leading edge of the plate; while it gradually decreases downstream and becomes the minimum. Comparatively, the pseudoplastic fluid decreases quickly near the leading edge but gradually increases downstream. Note that the skin-friction coefficient has the reverse phenomenon as shown in Fig. 7. These results may be explained as follows. As x increases, the free convection effect is cumulative and makes the flow accelerate, thereby causing a change of shear stress in non-Newtonian fluids. In Figs. 6

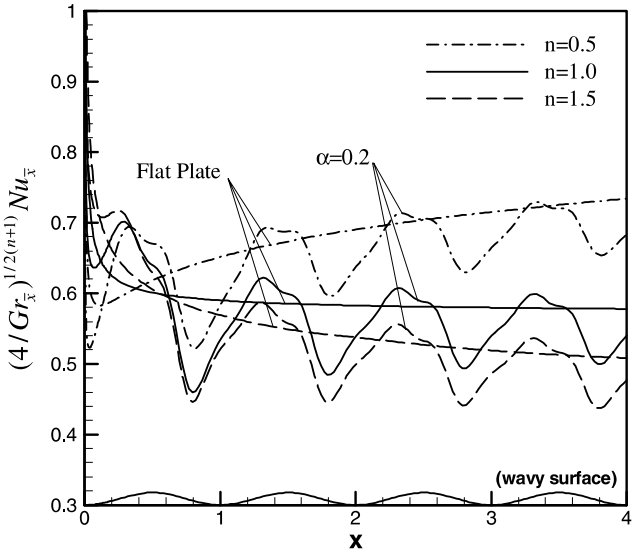

Fig. 6. Axial distribution of $(4/Gr_{\bar{x}})^{1/2(n+1)}Nu_{\bar{x}}$ for various values of power-law viscosity index with $\alpha = 0$ and 0.2, $Ri = 10$ and $Pr = 1$.

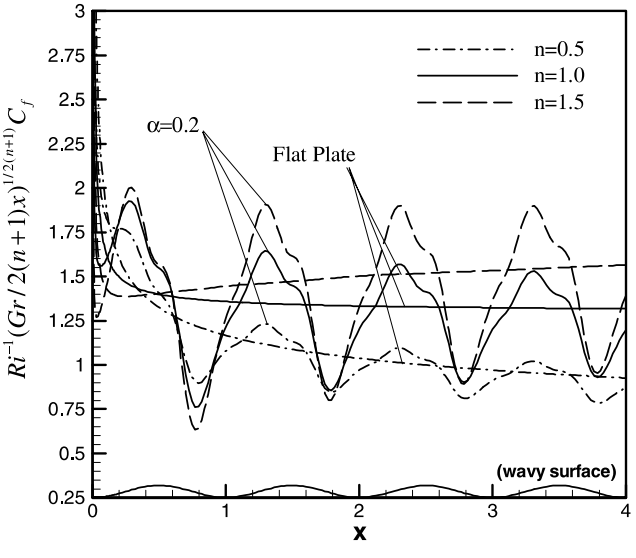

Fig. 7. Axial distribution of $Ri^{-1}(Gr/2(n+1)x)^{1/2(n+1)}C_f$ for various values of power-law viscosity index with $\alpha = 0$ and 0.2, $Ri = 10$ and $Pr = 1$.

and 7, we can also observe that the curves of $\alpha = 0.2$ show a frequency equals to that of the wavy surface for any fluid. It should be noted that the peaks of the local Nusselt number and the skin-friction coefficient occur

near the peaks of the wavy surface, where the inviscid free-stream velocity is maximum.

Figs. 8 and 9 also show variations of the local Nusselt number and the local skin-fiction coefficient for $\alpha = 0.2$, $Ri = 50$ and $Pr = 1$ and 10. In all cases, the presence of the second harmonic can be found in the curve for the Richardson number equals 50. This outcome is due to the lower axial velocity within the troughs of the wavy surface that exhibits higher temperature and greater sensitivity to the buoyancy force effect, thereby causing a larger change in velocity gradients at the wall. On the other hand, the wavy surface is seen to have a larger influence on the Nusselt number for higher generalized Prandtl number. Moreover, an increase in generalized Prandtl numbers decreases the quantity of skin-friction coefficient and increases that of heat transfer rate for any fluid.

The second harmonics of the local heat transfer rate and the skin-friction coefficient are seen more clearly near the troughs of the wavy surface in Figs. 10 and 11, in which the axial distributions of the local Nusselt number and the skin-friction coefficient are plotted for $Ri = 500$. In another word, the wavelengths of the local Nusselt number and the skin-friction coefficient are only half that of the wavy surface for larger Richardson numbers. This result is similar to that of free convection (see Kumari et al., 1997) except near the leading edge. Figs. 10 and 11 also observe that as wavy amplitude–wavelength ratios increase, the average quantities of Nusselt number and skin-friction coefficient decrease, even if both amplitudes increase for any fluid. For a given value of wavy amplitude–wavelength ratio, furthermore, the amplitude of skin-friction coefficient is seen to increase with the power-law viscosity index. But, this result is unobvious for the local Nusselt number.

The mean Nusselt number can be obtained by averaging the heat flux over the heat transfer area, which is based on the total area of each wave and not on projected area, from the leading edge to $\sigma(x)$, i.e.,

$$Nu_{\mathrm{m}} = \frac{h_{\mathrm{m}}\bar{\sigma}(\bar{x})}{K_{\mathrm{f}}} \tag{39}$$

where

$$h_{\mathrm{m}} = \frac{-1}{(T_{\mathrm{w}} - T_{\infty})\bar{\sigma}} \int_0^{\bar{x}} K_{\mathrm{f}} \frac{\partial T}{\partial n} \mathrm{d}\bar{\sigma} \tag{40}$$

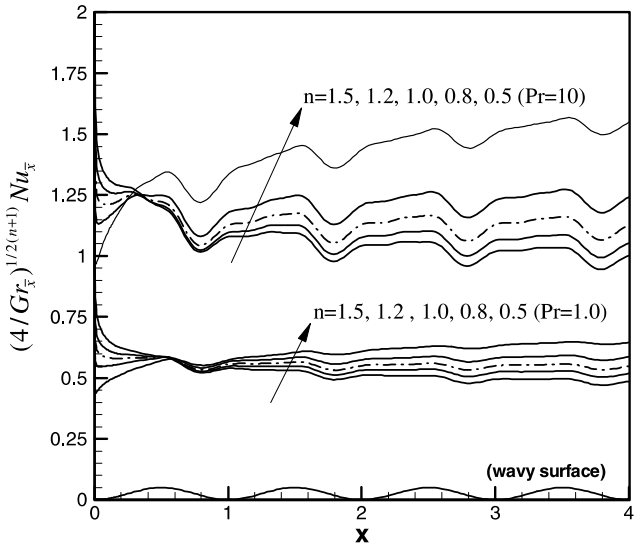

Fig. 8. Axial distribution of $(4/Gr_{\bar{x}})^{1/2(n+1)}Nu_{\bar{x}}$ for various values of power-law viscosity index and generalized Prandtl number with $\alpha = 0.2$, $Ri = 50$.

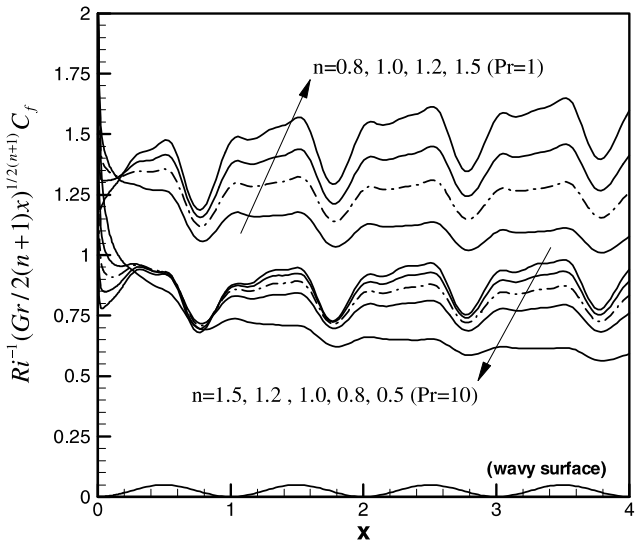

Fig. 9. Axial distribution of $Ri^{-1}(Gr/2(n+1)x)^{1/2(n+1)}C_{\mathrm{f}}$ for various values of power-law viscosity index and generalized Prandtl number with $\alpha = 0.2$, $Ri = 50$.

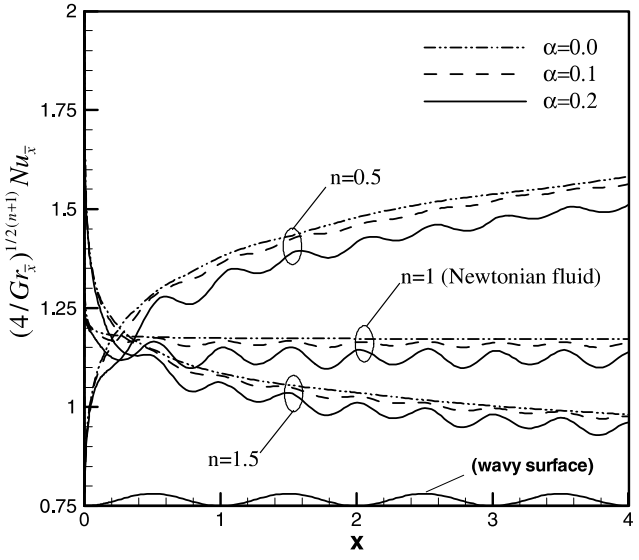

Fig. 10. Axial distribution of $(4/Gr_{\bar{x}})^{1/2(n+1)}Nu_{\bar{x}}$ for various values of power-law viscosity index and wavy amplitude–wavelength ratio with $Ri = 500$, $Pr = 1.0$.

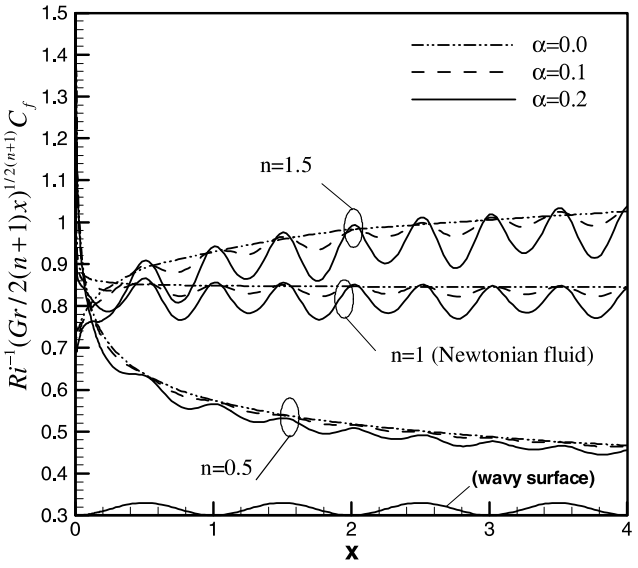

Fig. 11. Axial distribution of $Ri^{-1}(Gr/2(n+1)x)^{1/2(n+1)}C_f$ for various values of power-law viscosity index and wavy amplitude–wavelength ratio with $Ri = 500$, $Pr = 1.0$.

$$\bar{\sigma}(\bar{x}) = \int_0^{\bar{x}} (1 + \bar{S}'^2)^{1/2}\,\mathrm{d}\bar{x} \tag{41}$$

Then, the variation of $(4/Gr_{\bar{x}})^{1/2(n+1)}Nu_m$ with x, given by

$$\left(\frac{4}{Gr_{\bar{x}}}\right)^{1/2(n+1)} Nu_m = -\left(\frac{1}{Rix}\right)^{1/2(n+1)} \left(\frac{2}{x^n}\right)^{1/(n+1)} \times \int_0^x \left(\frac{U_w}{2x}\right)^{1/(n+1)} (1 + S'^2) \left.\frac{\partial\theta}{\partial y}\right|_{y=0} \mathrm{d}x \tag{42}$$

are plotted in Figs. 12–14 for $Ri = 10$, 50 and 500, respectively. Compare the mean Nusselt number with the

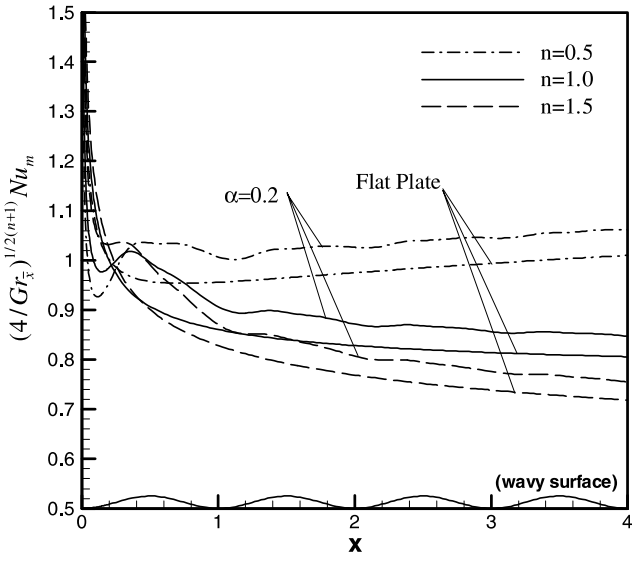

Fig. 12. Axial distribution of $(4/Gr_{\bar{x}})^{1/2(n+1)}Nu_m$ for various values of power-law viscosity index with $\alpha = 0$ and 0.2, $Ri = 10$ and $Pr = 1$.

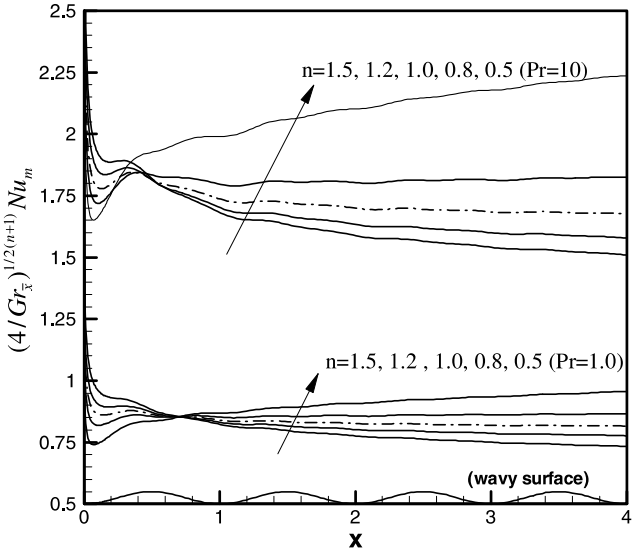

Fig. 13. Axial distribution of $(4/Gr_{\bar{x}})^{1/2(n+1)}Nu_m$ for various values of power-law viscosity index and generalized Prandtl number with $\alpha = 0.2$, $Ri = 50$.

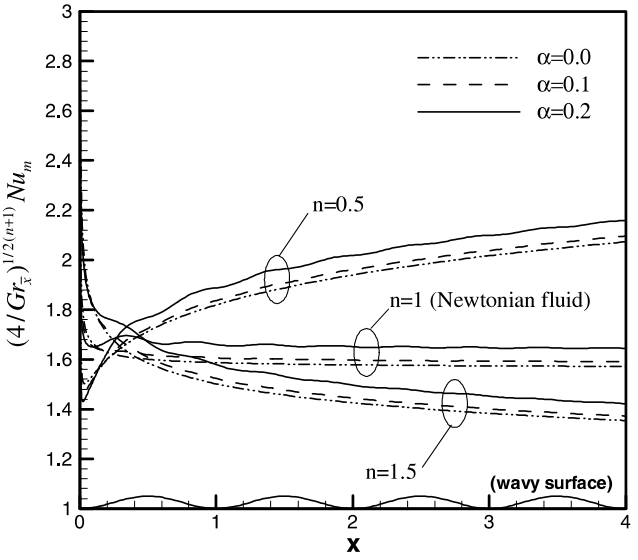

Fig. 14. Axial distribution of $(4/Gr_{\bar{x}})^{1/2(n+1)}Nu_m$ for various values of power-law viscosity index and wavy amplitude–wavelength ratio with $Ri = 500$, $Pr = 1.0$.

corresponding local Nusselt number (see Figs. 6, 8 and 10), it appears that the oscillations of $(4/Gr_{\bar{x}})^{1/4}Nu_m$ for the wavy plate show the same periodic behavior and have smaller amplitudes. Although the local Nusselt numbers of the wavy plate shown in Figs. 6 and 8 are almost everywhere smaller than that of the flat plate, the mean Nusselt number shown in Figs. 12 and 14 are uniformly larger than that of the corresponding flat plate. This indicates that the wavy plate has higher heat transfer rates than the corresponding flat plate for any fluid, which is due to the wavy plate has larger heat

transfer areas to raise the average heat transfer rate. Moreover, the increase in wavy amplitude–wavelength ratio is seen to enhance the mean heat transfer rate for difference fluids. On the other hand, the effects of generalized Prandtl number and power-law viscosity index in mean Nusselt number are also shown in Fig. 13. Clearly, the higher Prandtl number is seen to have the higher mean Nusselt number. Also, as power-law viscosity index increases, the mean Nusselt number increases near the leading edge and decreases far downstream of the leading edge. Note that the rate of decrease is more obvious for higher Prandtl numbers.

5. Conclusions

The analysis of laminar mixed convection heat transfer between a vertical wavy plate and non-Newtonian fluids has been presented. A square of sinusoid of surface is used to elucidate the effects of wavy amplitude–wavelength ratio, generalized Prandtl number and Richardson number for different fluids on the local Nusselt number, the mean Nusselt number and the skin-friction coefficient.

From the present results, it has been found that the behavior for non-Newtonian fluids near the leading edge of the wavy plate and downstream is quite different, i.e., the local and mean Nusselt numbers increase near the leading edge but decrease downstream with the power-law viscosity index. And this result is opposite for skin-friction coefficient. The wavy surface disturbs the flow and alters the heat transfer rate, thus makes the variations of the Nusselt number and the skin-friction coefficient on axial show a mixture of two harmonics for any fluid. The total heat transfer rate of the wavy surface is higher than that of the flat plate since the wavy surface has larger heat transfer areas. Also, both higher generalized Prandtl number and wavy amplitude wavelength ratio tend to enhance the total heat transfer for a given value of Richardson number.

References

Chiu, C.P., Chou, H.M., 1994. Transient analysis of natural convection along a vertical wavy surface in micropolar fluids. Int. J. Engng. Sci. 32, 19–33.

Hady, F.M., 1995. Mixed convection boundary-layer flow of non-Newtonian fluids on a horizontal plate. Appl. Math. Comput. 6, 105–112.

Huang, M.J., Chen, C.K., 1984. Numerical analysis for forced convection over a flat plate in power law fluids. Int. Commun. Heat Mass Transf. 11, 361–368.

Kim, E., 1997. Natural convection along a wavy vertical plate to non-Newtonian fluids. Int. J. Heat Mass Transf. 40, 3069–3078.

Kumari, M., Pop, I., Takhar, H.S., 1997. Free-convection boundary-layer flow of a non-Newtonian fluid along a vertical wavy surface. Int. J. Heat Fluid Flow 18, 625–631.

Lloyd, J.R., Sparrow, E.M., 1970. Combined forced and free convection flow on vertical surfaces. Int. J. Heat Mass Transf. 13, 434–438.

Moulic, S.G., Yao, L.S., 1989a. Natural convection along a vertical wavy surface with uniform heat flux. ASME J. Heat Transf. 111, 1106–1108.

Moulic, S.G., Yao, L.S., 1989b. Mixed convection along a vertical wavy surface. ASME J. Heat Transf. 111, 974–978.

Pop, I., Romania, C.S., Ohio, N.C., 1996. Laminar boundary layer flow of power-law fluids over wavy surfaces. Acta Mech. 115, 55–65.

Rees, D.A.S., Pop, I., 1994. A note on free convection along a vertical wavy surface in a porous medium. ASME J. Heat Transf. 116, 505–508.

Rubin, S.G., Graves, R.A., 1975. Viscous flow solution with a cubic spline approximation. Computers Fluids 1, 1–36.

Wang, T.Y., 1995. Mixed convection heat transfer from a vertical plate to non-Newtonian fluids. Int. J. Heat Fluid Flow 16, 56–61.

Wang, P., Kahawita, R., 1983. Numerical integration of partial differential equations using cubic spline. Int. J. Computer Math. 13, 271–286.